Atomic-scale perspective on individual thiol-terminated molecules anchored to single S vacancies in MoS_2

J. Rika Simon,[1] Dmitrii Maksimov,[2] Christian Lotze,[1] Paul Wiechers,[1] Juan Pablo Guerrero Felipe,[1] Björn Kobin,[3] Jutta Schwarz,[3] Stefan Hecht,[3,4] Katharina J. Franke,[1,*] and Mariana Rossi[2,†]

[1]*Fachbereich Physik, Freie Universität Berlin, 14195 Berlin, Germany*

[2]*Max Planck Institute for the Structure and Dynamics of Matter, 22761 Hamburg, Germany*

[3]*Institut für Chemie, Humboldt-Universität zu Berlin, 12489 Berlin, Germany*

[4]*Center for Science of Materials, 12489 Berlin, Germany*

(Received 1 April 2024; accepted 18 June 2024; published 3 July 2024)

Sulfur vacancies in MoS_2 on Au(111) have been shown to be negatively charged as reflected by a Kondo resonance. Here, we use scanning tunneling microscopy to show that these vacancies serve as anchoring sites for thiol-based molecules (CF_3-3P-SH) with two distinct reaction products, one of them showing a Kondo resonance. Based on comparisons with density-functional theory (DFT) calculations, including a random structure search and computation of energies and electronic properties at a hybrid exchange-correlation functional level, we conclude that both anchored molecules are charge neutral. We propose that one of them is an anchored intact CF_3-3P-SH molecule while the other one is the result of catalytically activated dehydrogenation to CF_3-3P-S with subsequent anchoring. Our investigations highlight a perspective of functionalizing defects with thiol-terminated molecules that can be equipped with additional functional groups, such as charge donor or acceptor moieties, switching units, or magnetic centers.

DOI: 10.1103/PhysRevB.110.045407

I. INTRODUCTION

Transition-metal dichalcogenides (TMDCs) are a class of materials with unwavering popularity for the last 50 years [1]. The recent interest in these materials originates from the possibilities of isolating single monolayers and stacking them in almost all imaginable ways, i. e., combining different materials, combining stacking orders, and rotations of the layers [2]. A single layer is distinct from its bulk counterpart in that the electronic band gap is changed due to confinement effects, e. g., transforming an indirect band gap to a direct one in MoS_2 [3,4].

The tunability of electronic properties through variable stacking allows for versatile applications in optoelectronics [5], in field effect transistors [6], in nanoelectromechanical systems [7], and in spintronics [8]. The two-dimensional (2D) nature of TMDCs does not only offer unprecedented flexibility, but also comes along with opportunities for device miniaturization [9,10].

Owing to the 2D nature, a small amount of defects already has a major effect on the electronic properties of the material. Often they introduce localized states inside the band gap of a semiconducting monolayer, which may be detrimental for certain applications, but also beneficial for others [11–15]. Attaining control over defects opens one more channel for tuning the local and global electronic properties of TMDCs, an area usually coined as defect engineering. The tunability can be enhanced even further by the functionalization of defects with molecular adsorbates [16–18]. This functionalization can lead to further possible charge transfer processes [19] and doping [20]. The hybrid systems may act as biosensors [21,22], and offer specific reaction sites [23].

Despite these fascinating opportunities, an atomistic understanding of the molecular functionalization in terms of the precise molecular configuration, the character of their bonding to the TMDC substrate and the resulting local electronic structure is largely in its infancy. In this paper, we study a molecular model system consisting of a thiol-terminated organic molecule and investigate its bonding properties to S vacancies in MoS_2. By combining scanning tunneling microscopy and theoretical modeling we gain fundamental insights into the atomic-scale bonding and electronic properties. We surmise that the understanding of this simple model system will form a basis for the design of future hybrid systems with more specific functions.

In more detail, we create S vacancies in the terminating S layer of MoS_2 on Au(111). The interaction of MoS_2 with the Au substrate has been shown to create negatively charged vacancies that localize a single electron at low temperatures [24]. Nevertheless, an analysis of defect formation energies suggests that a fraction of neutral vacancies can be present at higher temperatures [25,26]. In both scenarios, these sites

*Contact author: franke@physik.fu-berlin.de
†Contact author: mariana.rossi@mpsd.mpg.de

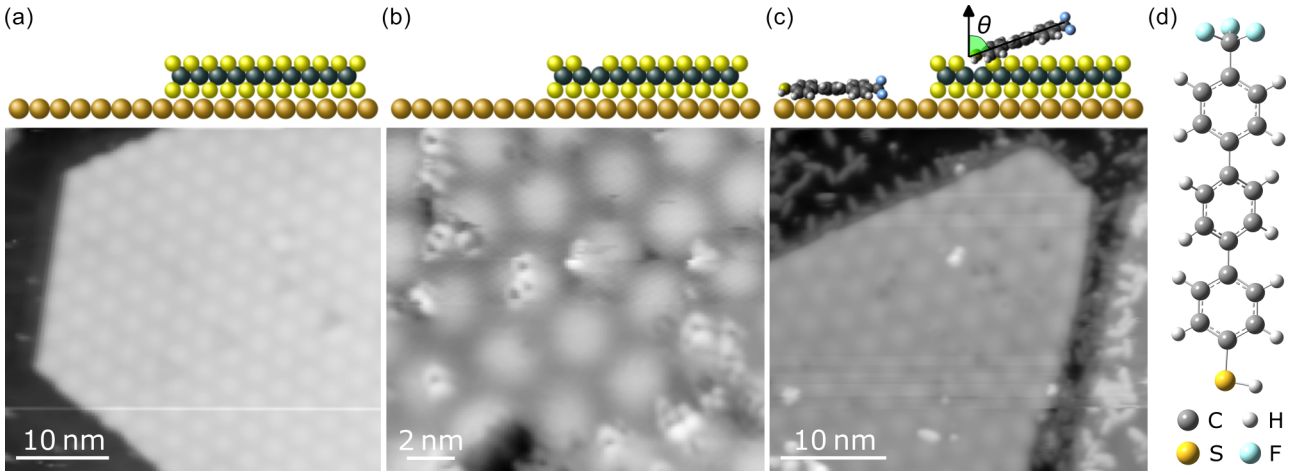

FIG. 1. Overview of STM topographies and illustrative sketches (not to scale) of the preparation steps: (a) MoS_2 on Au(111), showing the characteristic moiré pattern of the MoS_2 island (set point: 2 V, 200 pA). (b) Top-layer sulfur vacancies in MoS_2/Au(111), visible as triangular shapes, created by sputtering with Ne ions (set point: 50 mV, 200 pA). (c) CF_3-3P-S(H) on MoS_2/Au(111) after evaporation and subsequent annealing. Most CF_3-3P-S(H) molecules cluster together on the Au(111) surface, with only a few remaining on the MoS_2 island (set point: 2 V, 30 pA). We mark the tilting angle θ that defines the inclination of the molecule with respect to the surface normal on the inset. (d) Molecular model of CF_3-3P-SH in gas phase (gray: carbon; white: hydrogen; blue: fluorine; yellow: sulfur).

are expected to be highly reactive and ideal candidates for anchoring molecules. We expose these defects to 4″-(trifluoromethyl)-[1,1′:4′, 1″-terphenyl]-4-thiol (CF_3-3P-SH) molecules [Fig. 1(d)]. Thiol-based molecules are prone to covalently bind to S vacancies [20,27,28] and passivate them. In line with these expectations, we observe an anchoring of CF_3-3P-SH molecules to S defects on MoS_2/Au(111) and track the resulting changes in electronic structure in tunneling spectra.

We rationalize the resulting atomic and electronic structure by density-functional theory simulations. We find robust hybrid molecule-substrate localized electronic states and discuss the possibility of vacancies inducing a dehydrogenation of the molecule to CF_3-3P-S. We suggest that both the charged and neutral state of the S vacancy may play a role in the anchoring mechanism. However, regardless of the initial charge state of the vacancy, and whether dehydrogenation happens or not, a neutral anchored molecule is found to be the most stable state. This observation is compatible with two distinct experimentally observed molecular states, one of them exhibiting a Kondo resonance.

II. EXPERIMENTAL AND THEORETICAL DETAILS

The Au(111) surface was prepared for the MoS_2 growth by repeated cleaning cycles of sputtering and annealing under ultrahigh vacuum (UHV) conditions. A monolayer of MoS_2 was then grown on the atomically clean Au(111) substrate by depositing Mo atoms in an H_2S-atmosphere of 1×10^{-5} mbar onto the sample kept at 820 K [29,30]. The as-prepared sample was inspected in the STM to assure the successful formation of monolayer-islands of MoS_2 of about 100 nm in diameter. To remove any further adsorbates from the sample, we annealed it to 570 K. Sulfur vacancies were then introduced by sputtering with Ne ions (∼550 eV) at room temperature at a 45° angle for a few seconds. After confirming the presence of an appropriate density of S vacancies by STM (about 3–5 S vacancies in an area of $8 \times 10\,\mathrm{nm}^2$), CF_3-3P-SH molecules were evaporated from a Knudsen cell at an evaporation temperature of 365 K onto the MoS_2/Au(111) sample cooled to 160 K with subsequent annealing to 220 K. For details on the synthesis of the CF_3-3P-SH molecules, see Supplemental Material, Sec. SI [31]. All STM measurements were performed at 4.5 K under UHV conditions and dI/dV spectra were recorded using a standard lock-in technique.

For computational analysis, we conducted an exhaustive *ab initio* random structure search with the GENSEC package [32,33]. For molecular placement and distortion, random values were assigned to the internal torsional angles connecting the benzene rings of the molecule and to the orientation of the molecule with respect to the MoS_2 substrate. We constrained the search space by requiring that at least one atom of the molecule be placed at a distance of 3 Å from the defect site. A 6×6 unit cell containing one sulfur vacancy was assumed and, in the first step, no doping of the substrate was considered. Geometry relaxations were performed only on structures that met the criteria of no steric clashes according to a database of scaled van der Waals radii. The initial relaxations were performed with the PBE functional and MBD-NL van der Waals corrections [34], light settings in FHI aims [35], and a $1 \times 1 \times 1$ k grid. We conducted searches with the 3P-S molecule, the CF_3-3P-SH molecule and its dehydrogenated derivative, the CF_3-3P-S molecule. We optimized 35 structures of 3P-S, 45 structures of CF_3-3P-SH, and 75 structures of CF_3-3P-S in each search.

To increase the conformational diversity, we added CF_3 groups and H atoms to transform 3P-S molecules into CF_3-3P-S and CF_3-3P-SH and postrelaxed them. More details about the structure search can be found in the Supplemental Material [31], Sec. SII. We ended up with one candidate structure of CF_3-3P-SH and five candidate structures of CF_3-3P-S on MoS_2 that anchored on the defect. This subset of six

structures was further optimized with tight settings and a $4 \times 4 \times 1$ k grid, and then postoptimized with the HSE06 [36] functional with MBD-NL van der Waals corrections and intermediate settings of FHI aims [37]. The HSE06+MBD-NL functional relaxations were done on a $2 \times 2 \times 1$ k-point grid and we only required the forces to be below 10^{-2} eV/Å. Electronic structure properties and further analysis were all conducted at the HSE06 level of theory, including a post-processing spin-orbit coupling correction [38]. Some of these simulations were done with tight settings.

The same set of six conformers was reoptimized including a negative charge in the substrate, to model a negatively charged vacancy with charge −1. This was achieved by the use of a virtual-crystal approximation (VCA) scheme, as explained in Ref. [25]. We carried out geometry optimizations with the HSE06 functional with MBD-NL van der Waals corrections and intermediate settings, including the extra charge. Subsequently, electronic structure properties were analyzed at this level of theory, including the spin-orbit coupling correction.

While we did not include the Au slab explicitly in the simulations, we considered its effect implicitly in the calculation of binding energies and the estimation of charge states. Binding energies of anchored molecular structures under ultra-high-vacuum conditions (partial pressure tending to zero) were calculated by

$$E_b = E_{\text{anchor}}(q) - E_{\text{MoS}_2+\text{VS}}(q) - E_{\text{mol}} + qE_f^{\text{Au}}, \qquad (1)$$

where q is the charge, E_{anchor} is the total energy of the anchored molecular system, $E_{\text{MoS}_2+\text{VS}}$ is the total energy of the MoS_2 substrate containing the S vacancy, E_{mol} is the total energy of the CF_3-3P-SH molecule in the gas phase, and E_f^{Au} is the Fermi energy of Au. The total energies were obtained with the HSE06+MBD-NL functional and the Au Fermi energy at the HSE06 level of theory (−4.95 eV) was considered as an internally consistent reference. The value entering the computation was referenced to the position of the valence-band maximum (VBM) of the MoS_2 substrate containing the S vacancy at a consistent charge state and same DFT level of theory. With this definition, a more negative E_b means stronger binding. When the anchored molecule was dehydrogenated to CF_3-3P-S, we considered an adsorbed hydrogen far away from the defect site to obtain a simple estimate of a lower bound of the binding energy. We did not correct for finite-size effects.

III. ANCHORING CF_3-3P-SH MOLECULES TO S VACANCIES IN MoS_2

The pristine MoS_2 islands appear in STM topography with a characteristic moiré pattern caused by the lattice mismatch between MoS_2 and the underlying Au(111) [30] [Fig. 1(a)]. After sputtering with Ne ions, the MoS_2 layer is decorated with defects appearing with a triangular rim around a dark center [see Fig. 1(b)]. These defects have been attributed to S vacancies in the terminating S layer [24]. Importantly, at low temperatures these sites were shown to localize a single electron, which is exchange coupled to the metal electrons at the interface of MoS_2 and Au(111) as reflected by a Kondo resonance [24]. The localized negative charge is most likely transferred from the metal substrate. The observed charge state is in agreement with theoretical predictions, favoring the stabilization of the charged defect state in proximity to a Au substrate [25,39,40].

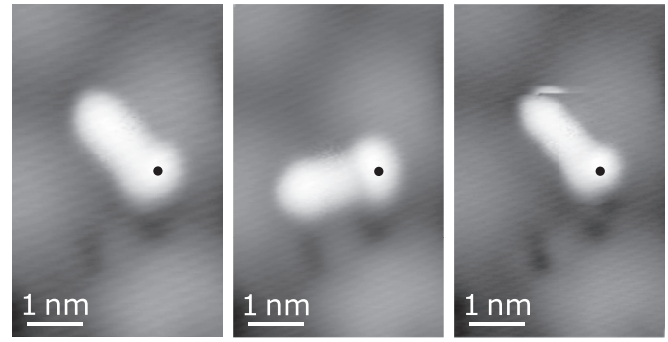

FIG. 2. STM topographies of subsequent rotation steps of a CF_3-3P-SH molecule on MoS_2/Au(111) around its anchoring point (marked by black dot) after interaction with the STM tip [set points: (a) and (c) 1 V, 40 pA, (b) 1 V, 50 pA].

Large organic molecules such as CF_3-3P-SH have a low diffusion barrier on MoS_2 [41]. To reduce diffusion and maintain a few molecules on the MoS_2 islands, a deposition temperature of 160 K was chosen. However, we then observed that most molecules were physisorbed on the islands with a very large mobility under the influence of the tip. Subsequent annealing to 220 K led to major diffusion, so that most of the CF_3-3P-SH molecules were found on the Au(111) substrate instead of on MoS_2. On Au(111) the molecules form clusters or are attached to the edges of the MoS_2 islands [Fig. 1(c)], most likely in a physisorbed configuration [42]). Yet, we also detected a few oval-shaped protrusions indicating single molecules on the MoS_2 substrate.

A close-up view on one of these molecules is shown in Fig. 2. Interestingly, the molecule is free to rotate around one of its terminations (indicated by a black dot in the series of images in Fig. 2). The rotations can be induced by approaching the STM tip. In none of the cases did the molecule move laterally. We thus assume that it is anchored to a defect site. Most probably, the defect is a S vacancy in the top layer of MoS_2, as we did not observe anchored CF_3-3P-SH molecules without prior creation of these sites by Ne bombardment. The robust anchoring of the molecule suggests the presence of a covalent bond to the S defect. Our preparation procedure of deposition at low temperature followed by mild annealing thus allows for some of the CF_3-3P-SH to bond to the S vacancies.

To unravel the atomic structure arising from this chemisorption scenario, we performed a combination of first-principles simulations. We analyzed the outcome of structure searches performed on a neutral and a negatively charged S-vacancy site in a freestanding monolayer of MoS_2 in contact with intact CF_3-3P-SH molecules and dehydrogenated CF_3-3P-S molecules. We considered both scenarios because in a previous publication from some of the authors [25], we have established that the formation energy difference between neutral and negatively charged vacancies only amounts to 43 meV when considering the Au substrate as the electronic reservoir. Therefore, by estimating the respective Boltzmann

weights, we conclude that while at very low temperatures one would exclusively observe charged vacancy sites, at the reaction temperature of 220 K, around 10% of these vacancy sites would be neutral.

When considering a negative charge, we did not obtain any CF_3-3P-SH molecules docked to the vacancy. In contrast, we obtained stable dehydrogenated CF_3-3P-S molecular configurations anchored to the defect site. This suggests that if the molecule docks, the H atom can be dissociated from the thiol group with the dangling bond at the S termination then being the ideal candidate for healing the S vacancy site in MoS_2. In the case of a neutral vacancy, both CF_3-3P-S and CF_3-3P-SH conformers are stable (see the Supplemental Material [31], Sec. SII).

Regarding the anchoring mechanism, we note that in order for CF_3-3P-S to bond to the vacancy site, a reaction barrier for dehydrogenation has to be overcome. We refer to the work of Li *et al.*, who characterized viable pathways for this reaction to happen at the defect site where the thiol group binds [28], reporting barriers of 0.2–0.3 eV. We conclude that this reaction can happen at neutral vacancies (available on the substrate at higher temperatures) and propose that these barriers can be lowered even further at negatively charged defects because these sites will be more attractive to protons. The abstracted H is likely to be highly mobile on MoS_2 and most probably diffuses to the metallic substrate. We surmise that a reaction, where H stays at a defect site and the unstable neutral radical diffuses and eventually finds another free defect site, is energetically highly unlikely. Indeed, negatively charged thiolates have been reported to be repelled even by neutral defects [28].

The local charge of the hybrid state formed by the molecule anchored to the defect site in MoS_2 is independent of whether the initial vacancy defect was neutral or negatively charged. Instead, it will be dictated by the stability of the hybrid state with respect to the electronic reservoir. Taking the electronic reservoir to be the Au substrate, we obtain the binding energy of the most favorable neutral conformer (considering CF_3-3P-SH and CF_3-3P-S) to be -0.56 eV, while the most favorable negatively charged case (considering only CF_3-3P-S, as the anchored CF_3-3P-SH is not stable in a negatively charged state) leads to a binding energy of only -0.08 eV, at the verge of stability within the uncertainties of our estimation. Note that the latter value does not include the energy penalty for dehydrogenation of CF_3-3P-SH into CF_3-3P-S. We did not explore positively charged final states because they would be even less likely in this setting. We thus propose that the final state of the anchored molecules is neutral. The structure of the negatively charged anchored molecules and the respective electronic states are presented in the Supplemental Material [31], Sec. SV, for completeness.

We now discuss the structural conformations of the anchored molecules. From the DFT simulations, the most stable CF_3-3P-SH conformer presents a tilting angle $\theta = 15^\circ$ with respect to the surface normal [see definition of θ in Fig. 1(c)]. Regarding the dehydrogenated CF_3-3P-S species, we found upright-standing configurations ($\theta \approx 0^\circ$) to be energetically favored. However, other stable minima within a 300 meV energy window are also found with larger θ (see the Supplemental Material [31], Sec. SII, Figs. S3– S6). In general, conformations with larger θ can be stabilized when considering entropic contributions. This was confirmed by exploratory molecular-dynamics simulations at 100–300 K, presented in the Supplemental Material [31], Sec. SIII. One can easily picture this, as any tilted configuration has access to a larger configurational space of rotations around the normal axis. Of course, we also cannot exclude that considering a lower concentration of molecules in the simulations can decrease the enthalpic penalty of tilted configurations, because it would decrease spurious interactions between periodic repetitions of the molecules. All geometries we obtain from the structure search, with and without H, present a lower θ than what experiment seems to observe, where the molecules are almost flat lying. In addition, we stress that in our simulations, several inclinations of the molecule are quite similar in energy (see the Supplemental Material [31], Sec. SII, Fig. S3), which suggests a very flat energy landscape along the inclination coordinate, such that we do not expect to be quantitative on the inclination angle based on static geometry optimizations.

In summary, we propose that, for either CF_3-3P-S or CF_3-3P-SH anchored to defect sites, two factors would contribute, if included in the simulations, to the stabilization of the tilted conformations with large θ which are observed experimentally: (i) a low concentration of molecules and (ii) entropic contributions that thermally populate the softer rovibrational modes of the molecule. We cannot exclude that a lowering of zero-point-energy contributions when molecular groups are physisorbed on the surface could also contribute to this stabilization.

IV. ELECTRONIC PROPERTIES OF ANCHORED MOLECULES

To investigate the electronic properties of the anchored molecules, we record dI/dV spectra on the anchored molecules. As we will show below, we found two types of dI/dV spectra. We investigated around 140 molecules and observed that 80% of them do not show a Kondo resonance while 20% do. We associate this electronic structure to two distinct molecules anchored to the S defects according to our theoretical simulations. One type consists of an intact CF_3-3P-SH molecule, whereas the other type has undergone dehydrogenation to a CF_3-3P-S molecule.

1. Anchored CF_3-3P-SH *molecules*

We start by presenting the dI/dV spectra on the more abundant species. Spectra on the anchoring site and the center of the molecule are shown in Fig. 3 (green and orange) together with a spectrum on the pristine MoS_2 (gray). In the latter, the conductance is essentially flat over a large bias-voltage range, in agreement with the semiconducting band gap of MoS_2, with the onset of the conduction band smeared out while exhibiting a small peak at ~ 0.9 V, followed by a stronger one at $\sim$1.4 V [41].

The anchored molecules show two main features inside the band gap of MoS_2 (Fig. 3): a positive ion resonance (PIR) of high intensity at ~ -1 V with satellite peaks following behind, and a broader negative ion resonance (NIR) starting at $\sim$420 mV. Both states are found to be very intense at the anchored end (green spectrum in Fig. 3), and show nearly

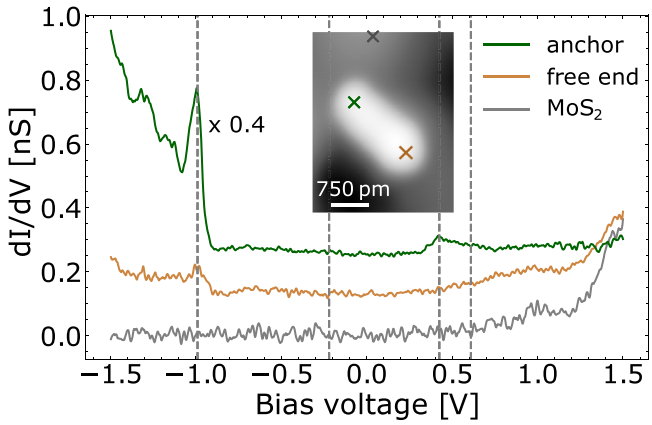

FIG. 3. dI/dV spectra on an anchored CF_3-3P-SH molecule on MoS_2/Au(111), on the anchor point (green), the free end (orange), and the reference taken on bare MoS_2 (gray). The spectra are vertically offset by 0.125 nS from each other. The spectrum on the anchored side has been rescaled by a factor of 0.4 for better comparison with the other spectra. The gray dashed lines denote the bias values of the dI/dV maps taken in Fig. 4. [Feedback opened at 1.5 V, 100 pA, lock-in parameters: 2 mV (MoS_2 and anchor) and 5 mV (free end) modulation amplitude.] Inset: STM topography of the measured molecule, with colored crosses marking the positions where the spectra are recorded (set point: 2 V, 30 pA). Note that the anchoring group of the molecule is located in a moiré minimum, while the free end is on a moiré maximum. The convolution of molecular and moiré states results in a featureless molecule at this bias voltage.

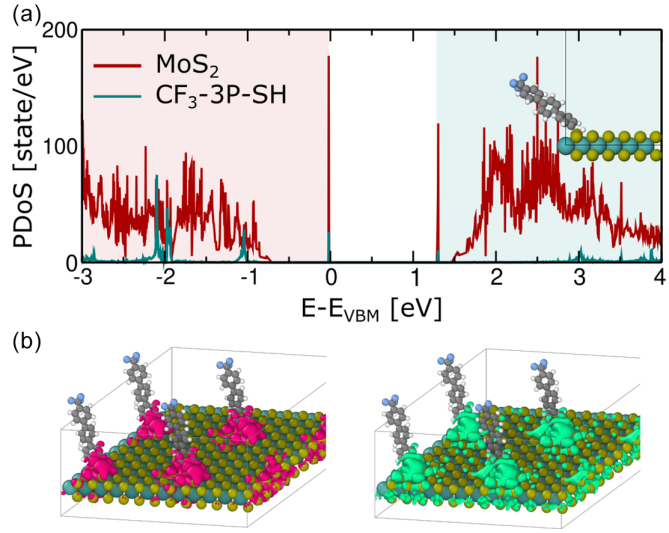

FIG. 5. (a) Projected electronic density of states (PDOS) of the stable conformer of CF_3-3P-SH anchored to the neutral MoS_2 monolayer, obtained with density-functional theory and the HSE06 exchange-correlation functional. The molecular geometry is shown in the inset. Cyan and red lines represent the PDOS on the molecule and on MoS_2, respectively. The red shaded area marks occupied states and the blue shaded area marks unoccupied states. The zero of energy is set to the valence band maximum (VBM) and that state is doubly occupied. (b) Orbital densities corresponding to the highest doubly occupied state in pink and the lowest unoccupied state in green. We show an isodensity of 0.0002 e/Bohr^3.

no intensity on the free end of the molecule (orange spectrum in Fig. 3). To bring out the spatial distribution of these states more clearly, we present constant-height dI/dV maps recorded at the resonance energies in Fig. 4 (energies of maps marked with a gray dashed line in Fig. 3).

The map taken at the energy of the PIR [−990 mV, Fig. 4(b)] shows a strong localization at the anchoring site. Additionally, it shows some faint intensity along the molecular backbone, exhibiting two nodal planes. The NIR at ∼420 mV also shows the largest contribution close to the anchoring site, but slightly offset from the molecular axis [Fig. 4(d)]. Maps at low energy [−220 meV, Fig. 4(c)] and higher energy [610 meV, Fig. 4(e)] show a faint structure along the molecule with some intramolecular modulation.

To understand the origin of the observed states, we analyze the electronic structure obtained by DFT calculations of candidate molecular configurations anchored on the S vacancy. We first consider the anchoring of an intact CF_3-3P-SH molecule on a neutral vacancy. This choice is motivated by the absence of a Kondo resonance, and, hence, of a singly occupied state.

In Fig. 5 we show the corresponding density of states of the CF_3-3P-SH molecule adsorbed on the vacancy. As we neglect the Au(111) substrate in the simulations, we do not expect quantitative agreement in the energy-level alignment but aim

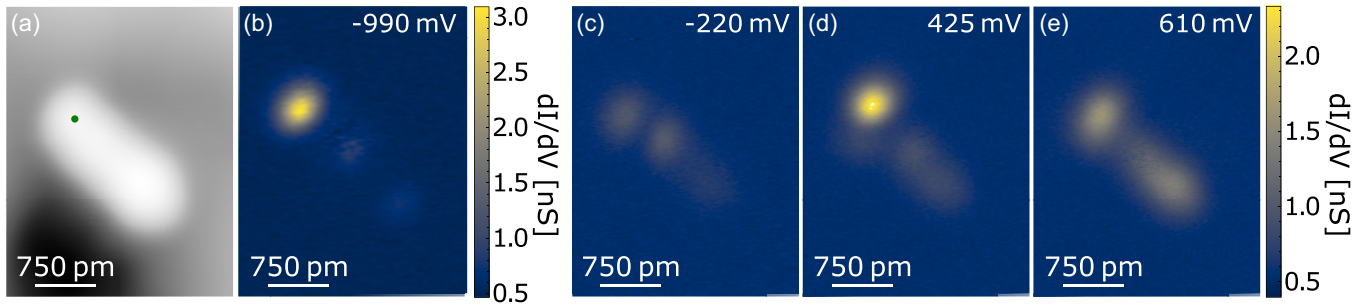

FIG. 4. (a) STM topography (set point: 2 V, 30 pA) and constant height dI/dV maps of an anchored CF_3-3P-SH molecule (anchor point marked by green dot) taken at energies marked by gray lines in Fig. 3: (b) −990 mV, (c) −220 mV, (d) 425 mV, (e) 610 mV. [Feedback opened at (b) −990 mV, 30 pA over anchored end, (c)–(e) 610 mV, 30 pA above free end, lock-in parameters for all: 5 mV modulation amplitude.]

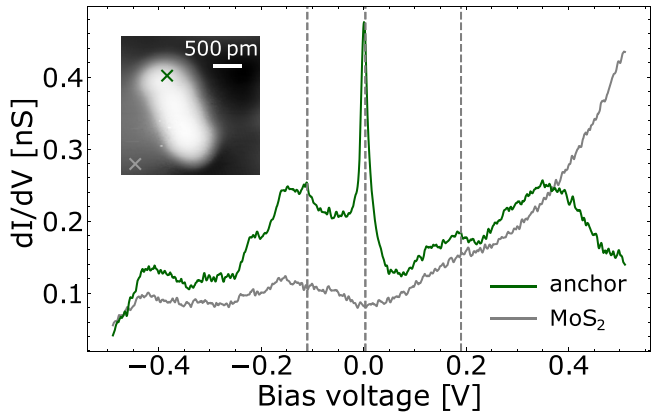

FIG. 6. dI/dV spectra on an anchored CF_3-3P-S molecule on MoS_2/Au(111), on the anchor point (green) and the reference taken on bare MoS_2 (gray). The gray dashed lines denote the bias values of the dI/dV maps shown in Fig. 7. (Feedback opened at 500 mV, 100 pA; lock-in parameters: 5 mV modulation amplitude.) Inset: STM topography of the measured molecule, with colored crosses marking the positions where the spectra were taken (set point: 1.3 V, 30 pA).

for a qualitative identification of the hybrid electronic states. In this case, both the highest (doubly) occupied state and the lowest unoccupied state are localized at the anchoring site. These states are separated by an energy gap of 1.3 eV. The states originate from the hybridization of the frontier orbitals of the CF_3-3P-SH molecule. In experiment, the energy separation of NIR and PIR is different from the HOMO-LUMO gap because of the charging energy necessary to transiently add and remove an electron from the system. In DFT, the Kohn-Sham states employing the hybrid exchange-correlation functional are only an approximation to HOMO and LUMO states. Nevertheless, as we only aim for a qualitative identification of the states, we consider the energy gap and the state localization to agree well between experiment and theory. We recall that for CF_3-3P-SH to bond to the defect site, the vacancy must be neutral. Although all pristine S vacancies exhibit a Kondo resonance at low temperatures reflecting a charged state, at the annealing temperature of 220 K the vacancy is transiently neutral with a relevant probability of 10%, as discussed above. The neutral state can thus act as an anchoring site for the intact CF_3-3P-SH molecule.

2. *Anchored dehydrogenated* CF_3-3P-S *molecules*

In contrast to the molecular species described above, we find a few molecules with a very different spectral fingerprint. As shown in Fig. 6, these molecules exhibit a sharp resonance at zero bias that we associate to a Kondo resonance flanked by two side peaks at ~ -110 mV and $\sim$190 mV. Differential conductance maps at these energies are presented in Fig. 7 along with the topographic image. All resonances are mainly localized at the anchoring site. Given their similar spatial distribution and close energy spacing, we suggest that the side peaks arise from tunneling through the singly occupied state at negative bias and the doubly occupied state separated by the Coulomb charging energy from the singly occupied state at positive bias. The experiments thus indicate the presence of a singly occupied state when the molecule is anchored to the S vacancy.

Following our stability analysis above, the hybrid state must be charge neutral, but a singly occupied state must be present. Therefore, we consider a dehydrogenated CF_3-3P-S radical bonded to the S vacancy. We suggest that H is catalytically dissociated from the thiol group when the molecule is in the vicinity of a negatively charged vacancy. The dangling bond is then saturated upon chemisorption of the CF_3-3P-S molecule to the vacancy site, and H could subsequently diffuse away from the anchored molecule. Because this incurs an energy penalty, this anchoring mode is less likely, in agreement with the less frequent observation as opposed to the first species discussed above. Overall charge neutrality results from the interaction of the Au substrate acting as a charge reservoir as discussed above. A representative molecular geometry, the projected electronic density of states and the visualization of key electronic states are shown in Fig. 8. The bonded conformations show a singly occupied state in the gap that could lead to a Kondo resonance. In agreement with experiment, this state is localized at the anchoring point. We also note that it is robust to several different molecular orientations found in the calculations. Other geometries with their corresponding electronic structure are reported in the Supplemental Material [31], Sec. SIV.

V. CONCLUSIONS

Using scanning tunneling spectroscopy, we have observed two types of reaction products of CF_3-3P-SH molecules

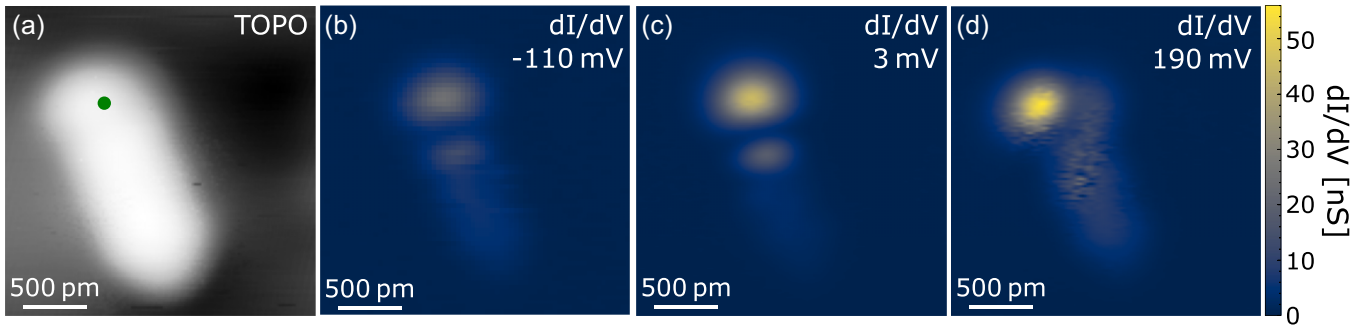

FIG. 7. (a) STM topography (set point: 1.3 V, 30 pA) and constant-height dI/dV maps of an anchored CF_3-3P-S molecule (anchor point marked by green dot) taken at energies marked by gray lines in Fig. 6. (b) −110 mV, (c) 3 mV, and (d) 190 mV. [Feedback opened at 500 mV, 100 pA, and 100 pm tip approach; lock-in parameters: 5 mV modulation amplitude.]

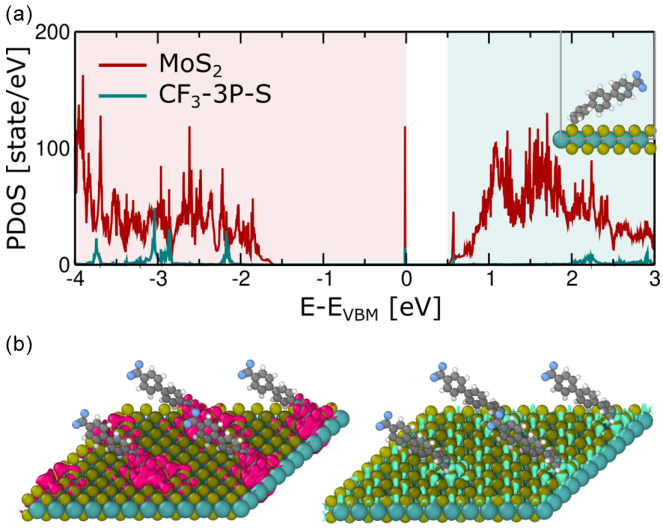

FIG. 8. (a) Projected electronic density of states (PDOS) of the stable conformer of CF_3-3P-S anchored to the neutral MoS_2 monolayer, obtained with density-functional theory and the HSE06 exchange-correlation functional. The molecular geometry is shown in the inset. Cyan and red lines represent the PDOS on the molecule and on MoS_2, respectively. The red shaded area marks occupied states and the blue shaded area marks unoccupied states. The zero of energy is set to the valence band maximum (VBM), and that localized state is singly occupied. (b) Orbital densities corresponding to the highest singly occupied state in pink and the lowest fully unoccupied state at 0.57 eV in green. We show an isodensity of 0.0002 e/Bohr^3.

anchoring to purposefully created S vacancies in MoS_2 on Au(111). Based on *ab initio* structure searches, DFT calculations, and comparison to the experimental tunneling spectra, we assign these two configurations to intact CF_3-3P-SH molecules or dehydrogenated CF_3-3P-S molecules and characterize their structural and electronic properties.

Due to the presence of the Au(111) substrate acting as a charge reservoir, both locally formed molecular hybrid states are charge neutral. Both species exhibit states within the band gap of MoS_2 and the anchored CF_3-3P-SH is more abundant. Interestingly, the CF_3-3P-S molecule features a singly occupied state, which explains the few anchored molecules that present a Kondo resonance in experiment. We note that the precise energy alignment and the localization of these new hybrid states depends sensitively on the adsorption configuration of the molecule on the moiré structure of MoS_2/Au(111) (see the Supplemental Material [31], Sec. SVI).

The combination of well-defined experiments and theory in this model system allowed an atomic-scale understanding of the properties of defect-engineered states, where a minimally biased first-principles structure search proved essential to unravel the possible atomic and electronic structure of docked molecules. Such an understanding would not be achievable with experiment or theory alone.

Going forward, the use of molecules with functional end groups, such as charge donating or charge withdrawing groups, will enable further modulation of the energy level alignment. Attachment of molecular switches may additionally allow a reversible variation of energy levels and, thus, conductance properties, while magnetic molecular centers may merge magnetic with the optoelectronic properties of the TMDC layer for more complex device applications.

The supporting data for this article are openly available from Zenodo [45].

ACKNOWLEDGMENTS

The authors thank Caterina Cocchi and Ana Valencia for discussions at an initial stage of this work, and Idan Tamir for technical support. We acknowledge funding by the Deutsche Forschungsgemeinschaft (DFG) through SFB 951 “Hybrid Inorganic/Organic Systems for Opto-Electronics” (Project No. 182087777, projects A13, A14, Z1).

[1] J. Wilson and A. Yoffe, The transition metal dichalcogenides: Discussion and interpretation of the observed optical, electrical and structural properties, Adv. Phys. **18**, 193 (1969).

[2] K. S. Novoselov, A. Mishchenko, A. Carvalho, and A. H. C. Neto, 2D materials and van der Waals heterostructures, Science **353**, aac9439 (2016).

[3] K. F. Mak, C. Lee, J. Hone, J. Shan, and T. F. Heinz, Atomically thin MoS_2: A new direct-gap semiconductor, Phys. Rev. Lett. **105**, 136805 (2010).

[4] A. Splendiani, L. Sun, Y. Zhang, T. Li, J. Kim, C. Chim, G. Galli, and F. Wang, Emerging photoluminescence in monolayer MoS_2, Nano Lett. **10**, 1271 (2010).

[5] M. Amani, D.-H. Lien, D. Kiriya, J. Xiao, A. Azcatl, J. Noh, S. R. Madhvapathy, R. Addou, S. KC, M. Dubey, K. Cho, R. M. Wallace, S.-C. Lee, J.-H. He, J. W. Ager, X. Zhang, E. Yablonovitch, and A. Javey, Near-unity photoluminescence quantum yield in MoS_2, Science **350**, 1065 (2015).

[6] B. Radisavljevic, M. B. Whitwick, and A. Kis, Integrated circuits and logic operations based on single-layer MoS_2, ACS Nano **5**, 9934 (2011).

[7] K.-A. N. Duerloo, M. T. Ong, and E. J. Reed, Intrinsic piezoelectricity in two-dimensional materials, J. Phys. Chem. Lett. **3**, 2871 (2012).

[8] Q. H. Wang, K. Kalantar-Zadeh, A. Kis, J. Coleman, and M. Strano, Electronics and optoelectronics of two-dimensional transition metal dichalcogenides, Nature Nanotechnol. **7**, 699 (2012).

[9] D. Joksas, A. AlMutairi, O. Lee, M. Cubukcu, A. Lombardo, H. Kurebayashi, A. J. Kenyon, and A. Mehonic, Memristive, spintronic, and 2D-materials-based devices to improve and complement computing hardware, Adv. Intell. Syst. **4**, 2200068 (2022).

[10] S. Salahuddin, K. Ni, and S. Datta, The era of hyper-scaling in electronics, Nature Electron. **1**, 442 (2021).

[11] Z. Yu, Y. Pan, Y. Shen, Z. Wang, Z.-Y. Ong, T. Xu, R. Xin, L. Pan, B. Wang, L. Sun, J. Wang, G. Zhang, Y. W. Zhang, Y. Shi, and X. Wang, Towards intrinsic charge transport in monolayer molybdenum disulfide by defect and interface engineering, Nature Commun. **5**, 5290 (2014).

[12] H. Nan, Z. Wang, W. Wang, Z. Liang, Y. Lu, Q. Chen, D. He, P. Tan, F. Miao, X. Wang, J. Wang, and Z. Ni, Strong photoluminescence enhancement of MoS_2 through defect engineering and oxygen bonding, ACS Nano **8**, 5738 (2014).

[13] Z. Lin, B. R. Carvalho, E. Kahn, R. Lv, R. Rao, H. Terrones, M. A. Pimenta, and M. Terrones, Defect engineering of two-dimensional transition metal dichalcogenides, 2D Mater. **3**, 022002 (2016).

[14] Q. Liang, Q. Zhang, X. Zhao, M. Liu, and A. T. S. Wee, Defect engineering of two-dimensional transition-metal dichalcogenides: Applications, challenges, and opportunities, ACS Nano **15**, 2165 (2021).

[15] S.-S. Chee, W.-J. Lee, Y.-R. Jo, M. K. Cho, D. Chun, H. Baik, B.-J. Kim, M.-H. Yoon, K. Lee, and M.-H. Ham, Atomic vacancy control and elemental substitution in a monolayer molybdenum disulfide for high performance optoelectronic device arrays, Adv. Funct. Mater. **30**, 1908147 (2020).

[16] Y. L. Huang, Y. J. Zheng, Z. Song, D. Chi, A. T. S. Wee, and S. Y. Quek, The organic-2D transition metal dichalcogenide heterointerface, Chem. Soc. Rev. **47**, 3241 (2018).

[17] S. Bertolazzi, M. Gobbi, Y. Zhao, C. Backes, and P. Samorì, Molecular chemistry approaches for tuning the properties of two-dimensional transition metal dichalcogenides, Chem. Soc. Rev. **47**, 6845 (2018).

[18] L. Daukiya, J. Seibel, and S. De Feyter, Chemical modification of 2D materials using molecules and assemblies of molecules, Adv. Phys.: X **4**, 1625723 (2019).

[19] S. Park, T. Schultz, X. Xu, B. Wegner, A. Aljarb, A. Han, L.-J. Li, V. C. Tung, P. Amsalem, and N. Koch, Demonstration of the key substrate-dependent charge transfer mechanisms between monolayer MoS_2 and molecular dopants, Commun. Phys. **2**, 109 (2019).

[20] S. M. Gali and D. Beljonne, Combined healing and doping of transition metal dichalcogenides through molecular functionalization, J. Mater. Chem. C **9**, 16247 (2021).

[21] H. Li, Z. Yin, Q. He, H. Li, X. Huang, G. Lu, D. W. H. Fam, A. I. Y. Tok, Q. Zhang, and H. Zhang, Fabrication of single- and multilayer MoS_2 film-based field-effect transistors for sensing NO at room temperature, Small **8**, 63 (2012).

[22] P. Fathi-Hafshejani, N. Azam, L. Wang, M. A. Kuroda, M. C. Hamilton, S. Hasim, and M. Mahjouri-Samani, Two-dimensional-material-based field-effect transistor biosensor for detecting COVID-19 virus (SARS-CoV-2), ACS Nano **15**, 11461 (2021).

[23] M. Asadi, K. Kim, C. Liu, A. V. Addepalli, P. Abbasi, P. Yasaei, P. Phillips, A. Behranginia, J. M. Cerrato, R. Haasch, P. Zapol, B. Kumar, R. F. Klie, J. Abiade, L. A. Curtiss, and A. Salehi-Khojin, Nanostructured transition metal dichalcogenide electrocatalysts for CO_2 reduction in ionic liquid, Science **353**, 467 (2016).

[24] S. Trishin, C. Lotze, N. Krane, and K. J. Franke, Electronic and magnetic properties of single chalcogen vacancies in MoS_2/Au(111), Phys. Rev. B **108**, 165414 (2023).

[25] A. Akkoush, Y. Litman, and M. Rossi, A hybrid-density functional theory study of intrinsic point defects in MX_2 (M = Mo,W; X = S,Se) monolayers, Phys. Stat. Sol. A **221**, 2300180 (2023).

[26] H.-P. Komsa and A. V. Krasheninnikov, Native defects in bulk and monolayer MoS_2 from first principles, Phys. Rev. B **91**, 125304 (2015).

[27] K. Cho, M. Min, T.-Y. Kim, H. Jeong, J. Pak, J.-K. Kim, J. Jang, S. J. Yun, Y. H. Lee, W.-K. Hong, and T. Lee, Electrical and optical characterization of MoS_2 with sulfur vacancy passivation by treatment with alkanethiol molecules, ACS Nano **9**, 8044 (2015).

[28] Q. Li, Y. Zhao, C. Ling, S. Yuan, Q. Chen, and J. Wang, Towards a comprehensive understanding of the reaction mechanisms between defective MoS_2 and Thiol Molecules, Angew. Chem., Int. Ed. **56**, 10501 (2017).

[29] S. S. Grønborg, S. Ulstrup, M. Bianchi, M. Dendzik, C. E. Sanders, J. V. Lauritsen, P. Hofmann, and J. A. Miwa, Synthesis of epitaxial single-layer MoS_2 on Au(111), Langmuir **31**, 9700 (2015).

[30] N. Krane, C. Lotze, and K. J. Franke, Moiré structure of MoS_2 on Au(111): Local structural and electronic properties, Surf. Sci. **678**, 136 (2018).

[31] See Supplemental Material at http://link.aps.org/supplemental/10.1103/PhysRevB.110.045407 for details on the synthesis of the CF_3-3P-SH molecules; more details about the structure search including energetic stability at several different inclination angles, details and analysis of *ab initio* molecular dynamics simulations, the structure of the negatively charged anchored molecules and the respective electronic states, different geometries of adsorbed CF_3-3P-S on a neutral substrate with their corresponding electronic structure, dI/dV spectra of different anchored CF_3-3P-SH, which includes Refs. [43,44].

[32] D. Maksimov and M. Rossi, sabia-group/gensec: Beta version of 2021, version (v0.0.0), Zenodo (2021), https://github.com/sabia-group/gensec, 10.5281/zenodo.5651512.

[33] D. Maksimov, Characterization and prediction of peptide structures on inorganic surfaces, Ph.D. thesis, IMX, 2022, https://doi.org/10.5075/epfl-thesis-9740.

[34] J. Hermann and A. Tkatchenko, Density functional model for van der Waals interactions: Unifying many-body atomic approaches with nonlocal functionals, Phys. Rev. Lett. **124**, 146401 (2020).

[35] V. Blum, R. Gehrke, F. Hanke, P. Havu, V. Havu, X. Ren, K. Reuter, and M. Scheffler, Ab initio molecular simulations with numeric atom-centered orbitals, Comput. Phys. Commun. **180**, 2175 (2009).

[36] A. V. Krukau, O. A. Vydrov, A. F. Izmaylov, and G. E. Scuseria, Influence of the exchange screening parameter on the performance of screened hybrid functionals, J. Chem. Phys. **125**, 224106 (2006).

[37] S. Kokott, F. Merz, Y. Yao, C. Carbogno, M. Rossi, V. Havu, M. Rampp, M. Scheffler, and V. Blum, Efficient all-electron hybrid density functionals for atomistic simulations beyond 10,000 atoms, J. Chem. Phys. (2024), doi: 10.1063/5.0208103.

[38] W. P. Huhn and V. Blum, One-hundred-three compound band-structure benchmark of post-self-consistent spin-orbit coupling treatments in density functional theory, Phys. Rev. Mater. **1**, 033803 (2017).

[39] A. M. Z. Tan, C. Freysoldt, and R. G. Hennig, Stability of charged sulfur vacancies in 2D and bulk MoS_2 from plane-wave density functional theory with electrostatic corrections, Phys. Rev. Mater. **4**, 064004 (2020).

[40] F. Tumino, C. S. Casari, A. L. Bassi, and S. Tosoni, Nature of point defects in single-layer MoS_2 supported on Au(111), J. Phys. Chem. C **124**, 12424 (2020).

[41] N. Krane, C. Lotze, G. Reecht, L. Zhang, A. L. Briseno, and K. J. Franke, High-resolution vibronic spectra of molecules on molybdenum disulfide allow for rotamer identification, ACS Nano **12**, 11698 (2018).

[42] A. K. Tuxen, H. G. Füchtbauer, B. Temel, B. Hinnemann, H. Topsøe, K. G. Knudsen, F. Besenbacher, and J. V. Lauritsen, Atomic-scale insight into adsorption of sterically hindered dibenzothiophenes on MoS_2 and Co-Mo-S hydrotreating catalysts, J. Catal. **295**, 146 (2012).

[43] G. Bussi, D. Donadio, and M. Parrinello, Canonical sampling through velocity rescaling, J. Chem. Phys. **126**, 014101 (2007).

[44] S. Trishin, C. Lotze, N. Bogdanoff, F. von Oppen, and K. J. Franke, Moiré tuning of spin excitations: Individual Fe atoms on MoS_2/Au(111), Phys. Rev. Lett. **127**, 236801 (2021).

[45] J. R. Simon, D. Maksimov, K. J. Franke, and M. Rossi, Data for "Atomic-scale perspective on individual thiol-terminated molecules anchored to single S vacancies in MoS_2" [Data set], Zenodo (2024), https://doi.org/10.5281/zenodo.10160204.